HHS Public Access

Author manuscript

Adv Mater. Author manuscript; available in PMC 2019 November 30.

Published in final edited form as:

Adv Mater. ; : e1706706. doi:10.1002/adma.201706706.

Inverse Opal Scaffolds with Gradations in Mineral Content for Spatial Control of Osteogenesis

Chunlei Zhu,
The Wallace H. Coulter Department of Biomedical Engineering, Georgia Institute of Technology and Emory University, Atlanta, GA 30332, USA

Jichuan Qiu,
The Wallace H. Coulter Department of Biomedical Engineering, Georgia Institute of Technology and Emory University, Atlanta, GA 30332, USA

Suphannee Pongkitwitoon,
Department of Orthopaedic Surgery, Columbia University, New York, NY 10032, USA

Stavros Thomopoulos, and
Department of Orthopaedic Surgery, Columbia University, New York, NY 10032, USA, Department of Biomedical Engineering, Columbia University, New York, NY 10027, USA

Younan Xia
The Wallace H. Coulter Department of Biomedical Engineering, Georgia Institute of Technology and Emory University, Atlanta, GA 30332, USA, School of Chemistry and Biochemistry, Georgia Institute of Technology, Atlanta, GA 30332, USA

Abstract

This paper describes the design and fabrication of inverse opal scaffolds with gradations in mineral content to achieve spatial control of osteogenesis. The gradient in mineral content was established *via* the diffusion-limited transport of hydroxyapatite nanoparticles in a closely-packed lattice of gelatin microbeads. The mineral-graded scaffold has an array of uniform pores and interconnected windows to facilitate efficient transport of nutrients and metabolic wastes, ensuring high cell viability. The graded distribution of mineral content can provide biochemical and mechanical cues for spatially regulating the osteogenic differentiation of adipose-derived stromal cells. This new class of scaffolds holds promise for engineering the interfaces between mineralized and unmineralized tissues.

Keywords

inverse opal scaffold; mineral gradient; osteogenesis; graded mineralization; interfacial tissue engineering

younan.xia@bme.gatech.edu.

Supporting Information

Supporting Information is available from the Wiley Online Library or from the author.

Human bodies rely on a number of musculoskeletal interfaces to transfer load between mineralized and unmineralized tissues, including the cartilage-bone (osteochondral), tendon-bone (tendon enthesis), and ligament-bone (ligament enthesis) joints.[1] The compliant-to-stiff transitional tissue typically exhibits gradations in mineral content, structural organization, cell phenotype, and extracellular matrix composition. The gradations are essential to functional integration between disparate tissues, minimization of stress concentrations, and efficient load transfer.[1,2] Owing to the limited regenerative capacity of these tissues after injury, surgical intervention is typically required to reattach the soft tissue to the bone in an attempt to restore joint function. Most surgical repairs, however, do not produce reliable clinical outcomes, primarily because the original functionally graded transitional tissue is not recreated.

In recent years, interfacial tissue engineering has emerged as a promising approach for the treatment of orthopedic tissue interfaces.[1] This strategy uses a cell-seeded three-dimensional (3D) scaffold to reproduce a robust interface between compliant and stiff tissues. To facilitate the regeneration of a functional tissue interface, several important criteria should be considered when designing and fabricating such a scaffold. First, the scaffold should have a porous structure to facilitate cell infiltration and proliferation. Second, spatially graded changes in biochemical and/or mechanical cues should be provided to generate a smooth transition between the dissimilar tissues. Third, the scaffold should be presented as a monolithic structure to ensure robust and seamless tissue integration. Although there are prior attempts to recapitulate the native mineral transition in orthopedic tissue interfaces,[1,3] most of the studies were focused on the fabrication of multilayered scaffolds rather than on creating monolithic structures. The major concern of these prior scaffolds lies in the abrupt boundaries between adjacent layers, which may not facilitate the formation of a smooth tissue interface. In addition, the layered scaffolds do not possess uniform porous structures, resulting in inhomogeneous mechanical properties within individual scaffolds and poor reproducibility across batches of scaffolds. The non-uniformity typically leads to insufficient local tissue formation, greatly limiting their applications in tissue regeneration. Inverse opal scaffolds, featuring a well-defined, highly ordered array of uniform and interconnected pores, have been actively explored for the repair/regeneration of bone, cartilage, and osteochondral tissues.[4] Owing to the uniform pores and interconnecting windows, as well as excellent reproducibility in physical properties across batches, they are emerging as ideal biomimetic substrates. However, these scaffolds have not been demonstrated for the promotion of a cell-phenotype gradient. As such, the emphasis of the current study was placed on the fabrication of inverse opal scaffolds with gradations in hydroxyapatite (HAp) mineral for achieving spatial control of osteogenesis of adipose-derived mesenchymal stem cells (ASCs). Since a large number of studies have demonstrated that the differentiation of stem cells can be controlled by substrate composition and stiffness,[5] we hypothesized that the osteogenic differentiation of ASCs should follow the pattern imposed by the mineral gradient. To our knowledge, this study describes the first inverse opal scaffold with smooth gradation in mineral content for spatial control of osteogenesis. We believe that this type of 3D scaffold will lead to a novel class of scaffolds and provide an important new tool for tissue engineering and regenerative medicine.

Scheme 1 illustrates the procedure used for fabricating the biodegradable inverse opal scaffold containing a mineral gradient. To ensure the translational potential of the scaffold, we only used materials approved by U.S. Food and Drug Administration (FDA), including poly(lactic-co-glycolic acid) (PLGA) and hydroxyapatite (HAp) mineral.[6] Uniform gelatin microbeads with an average diameter of *ca.* 200 μm were fabricated using a previously reported method.[7] We chose to focus on this size because the resulting porosity has been demonstrated to be optimal for cell migration, proliferation, and mineralization.[8] The gelatin microbeads were assembled into a cubic close packed (*ccp*) lattice in a centrifuge tube. Since the gelatin microbeads contained *ca.* 20–30 wt.% water, their glass transition temperature (60−120 °C) was much lower than that of dried gelatin (150−200 °C).[9] The centrifuge tube was pre-heated to 80 °C for 15 min to induce necking (partial fusion) between adjacent microbeads. A methanol suspension of the HAp nanoparticles (see Figure S1 for particle morphology) was then added into the centrifuge tube, followed by annealing at 80 °C for another 45 min. Driven by gravitational force, the HAp nanoparticles settled onto the top surface of the *ccp* lattice and entered into the void spaces among the gelatin microbeads. At the annealing temperature, the microbeads became soft and sticky. To minimize surface energy, the adjacent gelatin microbeads started to fuse. Meanwhile, the HAp nanoparticles stuck to the surface of the gelatin microbeads because of the increased adhesion. As nanoparticles penetrated into the *ccp* lattice, the pores at the top surface of the *ccp* lattice was gradually closed, limiting the transport of nanoparticles and thus facilitating the formation of a mineral gradient. Finally, the *ccp* lattice was infiltrated with a PLGA solution to fix the HAp nanoparticles trapped in the void spaces. After freeze-drying and removal of the gelatin template, a porous scaffold with a gradient in mineral content was obtained. It was noted that if the preheating time was longer than 30 min, the gelatin microbeads were subjected to dehydration with a hard and smooth surface. In this case, the HAp nanoparticles completely settled to the bottom of the lattice rather than forming a mineral gradient along the vertical direction. As such, the penetration depth of HAp through the gelatin particles could be modulated by varying the pre-heating time.

We used PLGA as the scaffolding material due to a number of advantages.[6a] First, PLGA is an FDA-approved biomaterial for clinical use, indicating its biocompatibility. Second, PLGA can provide appropriate mechanical properties and programmable biodegradability by varying the ratio of the two monomers (*i.e.,* lactic acid and glycolic acid). In this case, the degradation rate can be readily tuned to match the regeneration rate of target tissues, ultimately achieving a complete integration with the host. For other biomaterials, such as cross-linked collagen/gelatin, scaffold degradation would slowly release toxic cross-linking agents (*e.g.,* glutaraldehyde), resulting in adverse effects on tissue regeneration.[10] In addition, the use of collagen-based biomaterials risks immunogenic responses.[11] Based on these considerations, we chose to use PLGA for fabricating the HAp-graded inverse opal scaffolds.

Figure 1A shows a top-view scanning electron microscopy (SEM) image of a mineral-graded scaffold. The scaffold exhibited remarkable uniformity in terms of both pore size (179.4 ± 1.7 μm in diameter) and interconnecting window size (53.9 ± 2.3 μm in diameter). Owing to shrinkage of gelatin microbeads during solvent evaporation, the pore size of the scaffold was slightly smaller than that of the original microbeads. To quantify the mineral

distribution along the vertical direction, the scaffold was cryo-sectioned and then analyzed using energy-dispersive X-ray spectroscopy (EDX). As shown in Figure 1B, the atomic ratio of Ca to (Ca + C) gradually decreased as the layer number of pores increased. In the first layer, the ratio was as high as *ca.* 50%, whereas no calcium was detected in the regions furthest from the first layer. This trend in Ca content suggests a compositional gradient in mineral, confirming the successful incorporation of HAp nanoparticles into the backbone of the scaffold in a spatially graded fashion. To visualize the distribution of mineral content, micro-computed tomography (micro-CT) was used to characterize the scaffold (Figure 1C −F). A representative image shown in Figure 1C indicates that the scaffold had a cylinder-like shape, with diameters at the top and bottom surfaces being *ca.* 3 mm and 4 mm, respectively. From the enlarged image shown in Figure 1D, we observed a graded change in mineral content along the vertical direction. The bottom surface gave the highest image contrast, indicating the greatest accumulation of HAp mineral nanoparticles. The reconstructed 3D image was also vertically sectioned along the sagittal plane to reveal the spatial distribution of HAp nanoparticles inside the scaffold. The cross-sectional images shown in Figure 1, E and F, exhibited trends similar to those of the uncut scaffold except for the less prominent mineral contrast at the bottom surface, which can be attributed to excessive mineral deposition at the periphery of the *ccp* lattice during HAp sedimentation. Mean pixel intensity (MPI) analysis of the micro-CT images further confirmed the graded change in HAp density along the vertical direction (Figure S2). Taken together, these results demonstrate the successful fabrication of inverse opal scaffolds containing mineral gradients.

Since local mechanical properties play a crucial role in determining the fate of stem cells, we measured the Young's moduli at four locations along the mineral gradient of the HAp-graded scaffold using atomic force microscopy (AFM).[12] As shown in Figure 2, the Young's modulus decreased when the amount of HAp decreased along the mineral gradient, with the values changing from *ca.* 2 GPa to *ca.* 300 MPa. This gradient in mechanical properties is critical for alleviating stress concentrations at interfaces between dissimilar materials such as connective tissues and bone. For example, the moduli of a stiff material such as bone and a compliant material such as tendon are on the order of *ca.* 20 GPa and *ca.* 200 MPa, respectively.[2] As discussed in our prior publication,[12b] although the modulus in the mineralized region is one order of magnitude lower than that of bone, such a gap could be bridged *via* further biomineralization by the differentiated osteoblasts.

To examine the effect of the mineral-graded scaffold on cell behavior, ASCs, a promising source of mesenchymal stem cells capable of differentiating into multiple cell lineages, were seeded into the scaffold.[13] In contrast to mesenchymal stem cells derived from other sources, the ASCs offer many advantages for regenerative therapies.[14] First, they can be easily harvested using minimally invasive procedures. Second, they have the capability to differentiate into a variety of cell lineages. Third, they can be obtained in abundant quantities. Lastly, they display immunosuppressive properties and low immunogenicity. Previously, our group developed nanofiber-based scaffolds with gradations in HAp and studied their capacity for spatial control of osteogenesis.[14b] We found that HAp alone was able to encourage ASCs to differentiate into osteoblasts even in non-osteogenic medium. However, the differentiation process was slower and less significant than the case of

culturing ASCs in an osteogenic medium that was supplemented with β-glycerophosphate and ascorbic acid. Therefore, we decided to use the osteogenic medium to maximally induce the osteogenic differentiation of ASCs.

We first used a modified live/dead staining method to visualize cell viability and the distribution of ASCs inside the scaffold after 7, 14, and 21 days of culture. Since the inverse opal scaffold had a high porosity (*ca.* 74% relative to the entire volume), it was impossible to section the scaffold by direct cutting or liquid nitrogen cracking without destruction. To address this issue, we embedded the porous scaffold in optimal cutting temperature (OCT) compound, followed by cryo-sectioning along the vertical direction. Using this strategy, the original structure of the scaffold was largely preserved (Figure S3). Notably, OCT embedding reduced the fluorescence signal from the “live” indicator for the live/dead staining. Since nuclear staining was resistant to OCT embedding, we used a universal nuclear dye 4’,6-diamidino-2-phenylindole (DAPI) to reveal all cells and the “dead” indicator to identify dead cells, respectively. As shown in Figure 3A−C, the ASCs were attached along the wall of the pore and homogeneously distributed inside the scaffold at all time points. More importantly, the ASCs remained viable at all locations inside the scaffold, regardless of mineral content. Further analysis indicated that the survival rates of ASCs after 7, 14, and 21 days of culture were 94.7 ± 0.7, 95.2 ± 1.2, and 95.7 ± 1.4%, respectively (Figure 3D). This result suggests excellent biocompatibility for the mineral-graded scaffolds. The uniform and interconnected pore structure of the inverse opal scaffold indeed enabled the efficient transport of nutrients and metabolic wastes, leading to homogenous cell distribution and high cell viability.

To examine the impact of mineral gradation on the differentiation of ASCs, osteogenesis was examined after 7, 14, and 21 days of culture. Alkaline phosphatase (ALP) is an enzyme required for cartilage and bone mineralization. It is expressed by differentiating osteoblasts so it can be considered an early marker of osteogenesis.[15] During mineralization, ALP hydrolyzes organic phosphate esters into free inorganic phosphate to initiate the deposition of HAp on extracellular proteins. A commercial staining kit was used to assess ALP activity in the current study. The as-obtained images were then vertically divided into five locations to analyze the corresponding MPI (Figure 4). At day 7, ALP expression was only observed at locations 4 and 5, corresponding to the regions with relatively high mineral contents (Figure 4A). In contrast, no noticeable signal was detected at locations 1–3, corresponding to regions with low HAp contents. Quantitative intensity analysis showed no significant differences among locations 1–3 (Figure 4D). At day 14, there was an increase in ALP expression compared to day 7, and fluorescence at locations 1−3 became apparent, suggesting a gradual increase in ALP activity (Figure 4, B and E). More importantly, a gradient in fluorescence intensity became prominent, positively correlated with the spatial distribution of HAp nanoparticles. At day 21, a gradient in ALP expression remained. There was only a slight increase in fluorescence intensity at day 21 compared to day 14, suggesting that stable levels of spatially controlled ALP expression were achieved by day 14 (Figure 4, C and F). In addition, a large number of bone-like nodules were seen in the scaffold, supporting the conclusion of successful mineralization by ASCs (Figure 4, B and C).[16]

To further evaluate osteogenesis on the mineral-graded scaffolds, immunocytochemical staining was performed for osteocalcin (OCN) after 14 and 21 days of culture. OCN, a non-collagenous protein found in bones, is a specific marker of osteoblasts and thus considered a late marker of osteogenic differentiation (Figure 5, A and B).[17] To better present the localized expression of OCN by ASCs, images were taken at four locations. At day 14, only weak fluorescence was detected at locations 1 and 2, corresponding to regions with low HAp contents. In contrast, positive staining became evident at locations 3 and 4. Quantitative analysis of MPI at locations 1−4 indicated that there was a graded change in fluorescence intensity; this was positively correlated with the mineral gradient (Figure 5C). At day 21, all locations exhibited stronger fluorescence compared to those at day 14, and the fluorescence gradient from locations 1–4 became more evident (Figure 5D). Owing to the capacity to promote osteogenesis both *in vitro* and *in vivo*, HAp is considered an osteoconductive and osteoinductive material.[18] Because stem cells are able to respond to both biochemical and mechanical cues, the substrates with increased mineral content facilitated the differentiation of ASCs.

To visualize the spatial mineralization of ASCs, Alizarin Red S was used to evaluate the calcium-rich deposits at day 21. For comparison, the as-prepared, cell-free scaffold (day 0) was used as a control. As shown in Figure 6A, only the bottom section of the scaffold was stained red, whereas the top section maintained its original white color. Although Alizarin Red S staining was not able to reveal all HAp nanoparticles, particularly for those embedded in the scaffold backbone, the overall trend in calcium content could be resolved. At day 21, the entire section showed a stronger positive staining than the control sample, and the graded change in red color became more apparent (Figure 6B). In addition, bone-like nodules were observed, as indicated by the white arrowheads. This result suggests that, after 21 days of culture, the seeded ASCs exhibited a phenotypic change toward osteogenesis and then mineralization. More importantly, the osteogenic and mineralization pattern was dictated by the gradient in HAp nanoparticles. It should be pointed out that in addition to the newly produced calcium deposits, Alizarin Red S will also stain the original HAp nanoparticles doped in the as-prepared scaffold. In order to quantify such a difference, we performed MPI analysis to evaluate the mineralization process. Since calcium staining by Alizarin Red S led to a significant decrease in MPI, the difference in MPI could be used as an indicator for additional biomineralization. As shown in Figure 6C, the MPIs for the scaffolds at both 0 and 21 days exhibited a graded decrease from locations 1 to 5. Nevertheless, the decrease in MPIs was significantly strengthened at day 21, indicating the positive effect of mineral gradient on the graded mineralization of ASCs. In addition, in contrast to the as-prepared scaffolds at day 0, biomineralization promoted the formation of a smoother gradient in mineral content, indicating its potential for re-establishing a smooth mineral interface.

In conclusion, we have developed a simple and versatile method for fabricating inverse opal scaffolds with gradations in mineral content for spatial control of osteogenesis. The seeded ASCs exhibited differential responses to the resultant scaffold with graded changes in biochemical and mechanical cues. The biocompatible scaffold provided an appropriate microenvironment to favor efficient transport of nutrients and metabolic wastes, enabling the seeding of ASCs and maintenance of high cell viability during culture. Owing to the osteoconductivity and osteoinductivity of HAp, the expression of both early (ALP) and late

(OCN) makers for osteogenesis was found to be positively correlated with the graded change in mineral content. More importantly, the gradient in cell phenotypes could recapitulate the cellular pattern seen in many connective tissue-to-bone interfaces. This study offers a strategy for engineering tissue interfaces by introducing gradients in both mineral content and cell type. This approach can also be integrated with various bioactive molecules (*e.g.*, growth factors) and/or nanostructures (*e.g.*, aligned nanofibers) to further facilitate seamless integration between adjoining tissues, holding great promise for orthopedic interface regeneration.

Supplementary Material

Refer to Web version on PubMed Central for supplementary material.

Acknowledgements

C.Z., J.Q., and S.P. contributed equally to this work. This work was supported in part by a grant from the National Institutes of Health (R01 AR060820) and startup funds from the Georgia Institute of Technology.

References

[1] a). Cross LM, Thakur A, Jalili NA, Detamore M and Gaharwar AK, Acta Biomater 2016, 42, 2 [PubMed: 27326917]

b). Qu D, Mosher CZ, Boushell MK, Lu HH, Ann. Biomed. Eng 2015, 43, 697 [PubMed: 25465616]

c). Yang PJ, Temenoff JS, Tissue Eng. Part B Rev 2009, 15, 127. [PubMed: 19231983]

[2]. Lu HH, Thomopoulos S, Annu. Rev. Biomed. Eng 2013, 15, 201. [PubMed: 23642244]

[3] a). Atesok K, Doral MN, Karlsson J, Egol KA, Jazrawi LM, Coelho PG, Martinez A, Matsumoto T, Owens BD, Ochi M, Hurwitz SR, Atala A, Fu FH, Lu HH, Rodeo SA, Knee Surg. Sports Traumatol. Arthrosc 2016, 24, 2365 [PubMed: 25466277]

b). Dormer NH, Berkland CJ, Detamore MS, Ann. Biomed. Eng 2010, 38, 2121. [PubMed: 20411333]

[4] a). Zhang YS, Choi SW, Xia Y, Soft Matter 2013, 9, 9747

b). Zhang YS, Zhu C, Xia Y, Adv. Mater 2017, 29, 1701115.

[5] a). Macrí-Pellizzeri L, Pelacho B, Sancho A, Iglesias-García O, Simón-Yarza AM, Soriano-Navarro M, González-Granero S, García-Verdugo JM, De-Juan-Pardo EM, Prosper F, Tissue Eng. Part A 2015, 21, 1633 [PubMed: 25668195]

b). Lee J, Abdeen AA, Zhang D, Kilian KA, Biomaterials 2013, 34, 8140. [PubMed: 23932245]

[6] a). Gentile P, Chiono V, Carmagnola I, Hatton PV, Int. J. Mol. Sci 2014, 15, 3640 [PubMed: 24590126]

b). Loghem JV, Yutskovskaya YA, Philip Werschler W, J. Clin. Aesthet. Dermatol 2015, 8, 38.

[7]. Choi SW, Cheong IW, Kim JH, Xia Y, Small 2009, 5, 454. [PubMed: 19189332]

[8] a). Choi SW, Zhang Y, Xia Y, Langmuir 2010, 26, 19001 [PubMed: 21090781]

b). Choi SW, Zhang Y, Thomopoulos S, Xia Y, Langmuir 2010, 26, 12126. [PubMed: 20450216]

[9]. Zhang YS, Regan KP, Xia Y, Macromol. Rapid Commun 2013, 34, 485. [PubMed: 23365045]

[10] a). Bigi A, Cojazzi G, Panzavolta S, Rubini K, Roveri N, Biomaterials 2001, 22, 763 [PubMed: 11246944]

b). Tondera C, Hauser S, Krüger-Genge A, Jung F, Neffe AT, Lendlein A, Klopfleisch R, Steinbach J, Neuber C, Pietzsch J, Theranostics 2016, 6, 2114. [PubMed: 27698944]

[11]. Parenteau-Bareil R, Gauvin R, Berthod F, Materials 2010, 3, 1863.

[12] a). Pongkitwitoon S, Uzer G, Rubin J, Judex S, Sci. Rep 2016, 6, 34791 [PubMed: 27708389]

b). Zhu C, Pongkitwitoon S, Qiu J, Thomopoulos S, Xia Y, Adv. Mater 2018, DOI: 10.1002/adma.201707306.

[13] a). Dai R, Wang Z, Samanipour R, Koo KI, Kim K, Stem Cells Int 2016, 2016, 6737345 [PubMed: 27057174]

b). Shen H, Gelberman RH, Silva MJ, Sakiyama-Elbert SE, Thomopoulos S, PLoS One 2013, 8, e77613. [PubMed: 24155967]

[14] a). Frese L, Dijkman PE, Hoerstrup SP, Transfus. Med. Hemother 2016, 43, 268 [PubMed: 27721702]

b). Liu W, Lipner J, Xie J, Manning CN, Thomopoulos S, Xia Y, ACS Appl. Mater. Interfaces 2014, 6, 2842. [PubMed: 24433042]

[15] a). Marom R, Shur I, Solomon R, Benayahu D, J. Cell Physiol 2005, 202, 41 [PubMed: 15389528]

b). Golub EE, Boesze-Battaglia K, Curr. Opin. Orthopaed 2007, 18, 444.

[16]. Aiami SM, Gangloff SC, Laurent-Maquin D, Wang Y, Kerdjoudj H, Stem Cell Trans. Med 2016, 5, 1587.

[17] a). Ayukawa Y, Takeshita F, Inoue T, Yoshinari M, Shimono M, Suetsugu T, Tanaka T, J. Biomed. Mater. Res 1998, 41, 111 [PubMed: 9641631]

b). Lee NK, Sowa H, Hinoi E, Ferron M, Ahn JD, Confavreux C, Dacquin R, Mee PJ, Mckee MD, Jung DY, Zhang Z, Kim JK, Mauvais-Jarvis F, Ducy P, Karsenty G, Cell 2007, 130, 456. [PubMed: 17693256]

[18] a). Kang R, Luo Y, Zou L, Xie L, Lysdahl H, Jiang X, Chen C, Bolund L, Chen M, Besenbacher F, Bünger C, RSC Adv 2014, 4, 5734

b). Gao X, Song J, Ji P, Zhang X, Li X, Xu X, Wang M, Zhang S, Deng Y, Deng F, Wei S, ACS Appl. Mater. Interfaces 2016, 8, 3499. [PubMed: 26756224]

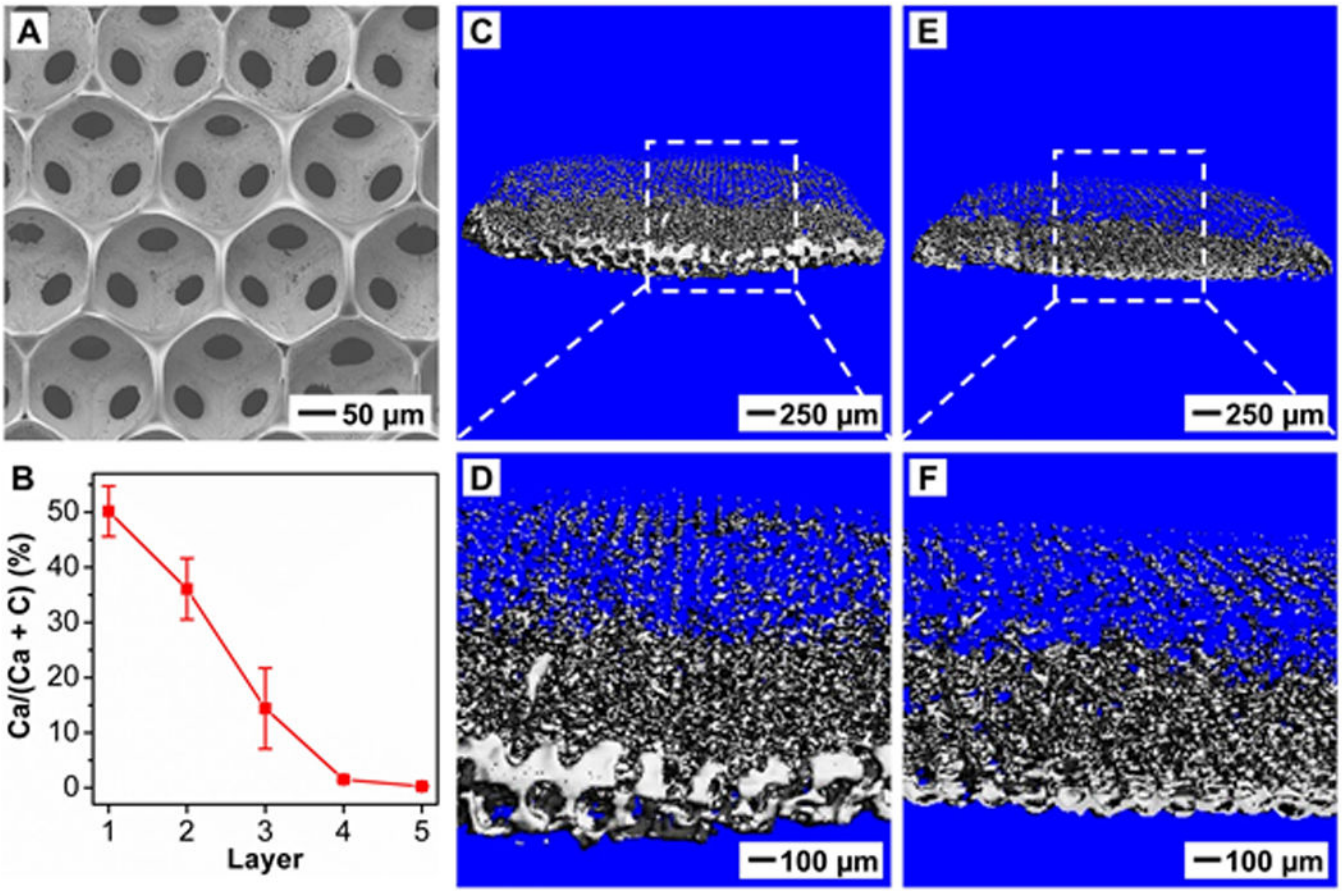

Figure 1.

Characterization of the distribution of HAp nanoparticles in the PLGA inverse opal scaffold. A) Top-view SEM image. B) EDX quantification of calcium content along the vertical direction ($n = 3$). The layer number refers to the layer of pores after template removal (see Scheme 1). C−F) Micro-CT images of (C, D) an HAp-graded PLGA scaffold and (E, F) its sagittal sectioning plane.

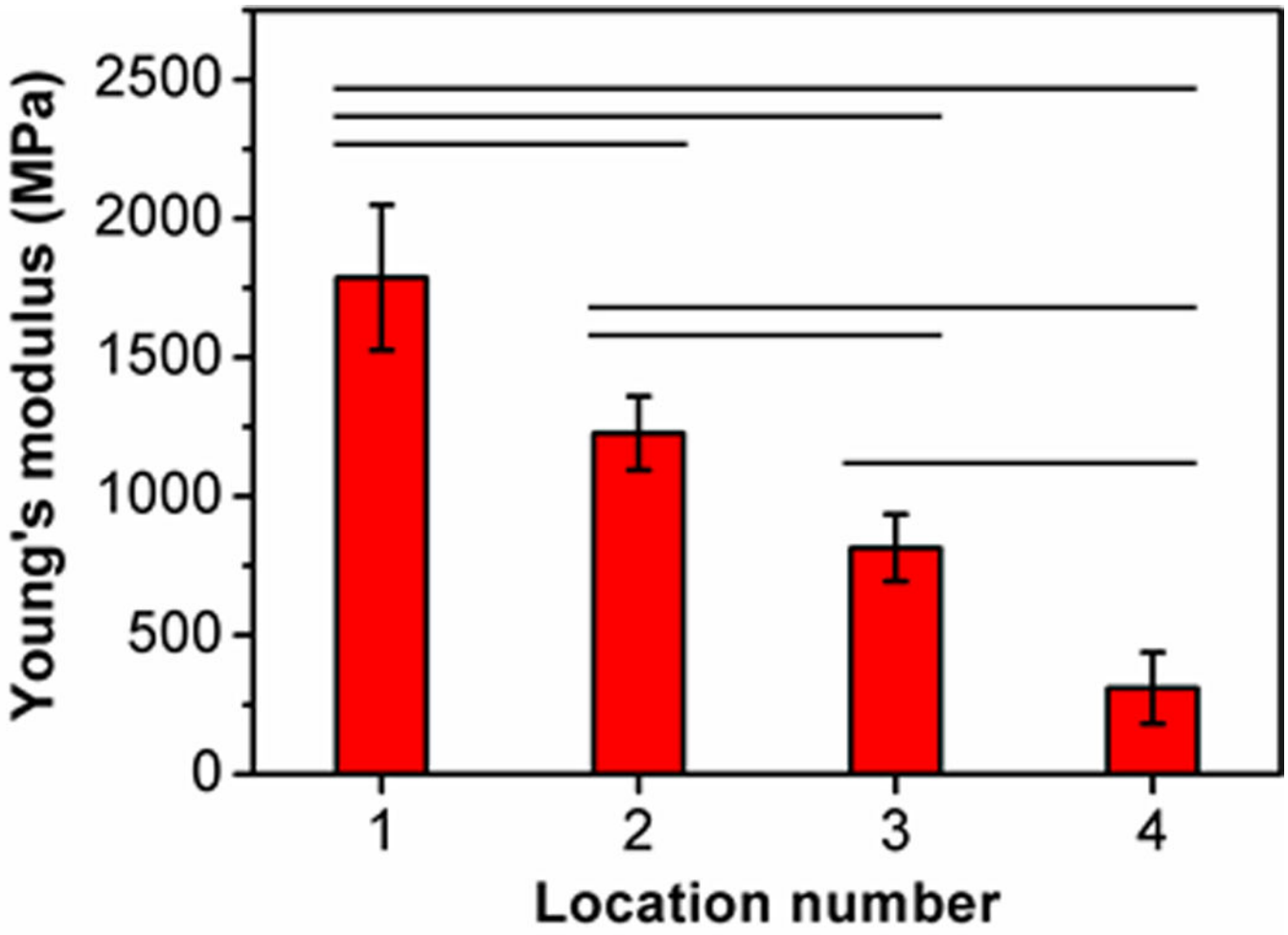

Figure 2.

Local Young's modulus in the HAp-graded PLGA inverse opal scaffold. The modulus was measured in four locations along the mineral gradient (location numbers 1 and 4 represent highly mineralized and unmineralized regions, respectively) ($n = 6$). Significant differences are indicated by lines over the bars ($p < 0.05$).

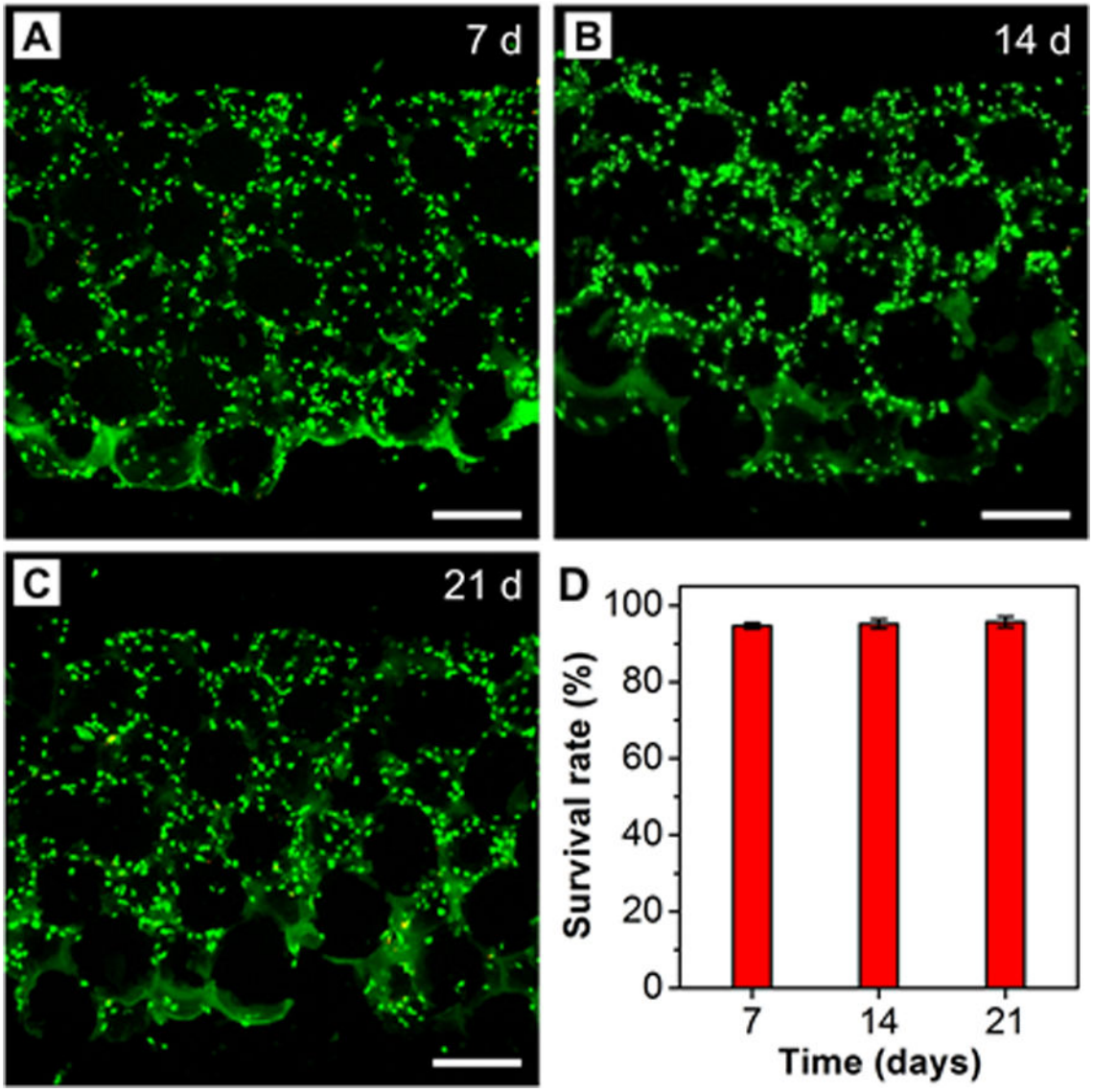

Figure 3.

Live/dead staining of ASCs seeded in the HAp-graded PLGA inverse opal scaffolds after A) 7, B) 14, and C) 21 days of culture. DAPI is highlighted in green to reveal the location of ASCs. Scale bars: 200 μm. D) Cell survival rates derived from images such as those shown in (A–C) ($n = 3$).

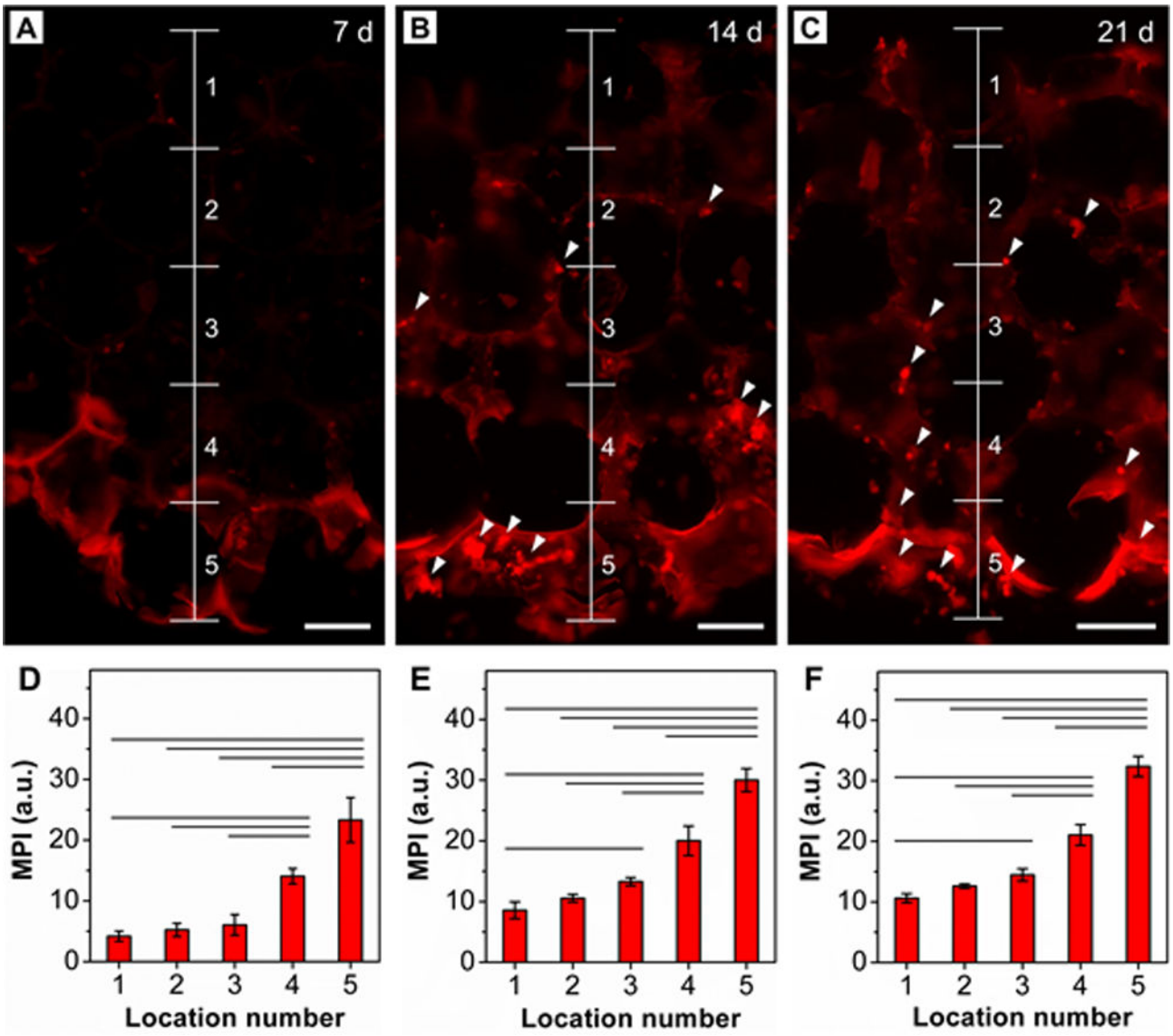

Figure 4.

ALP staining (red) of ASCs seeded in the HAp-graded PLGA inverse opal scaffold after A) 7, B) 14, and C) 21 days of culture. White arrowheads indicate the calcium nodules. Scale bars: 100 μm. D−F) MPI analysis of ALP along the vertical direction after D) 7, E) 14, and F) 21 days of culture ($n = 3$). Significant differences are indicated by lines over the bars ($p < 0.05$).

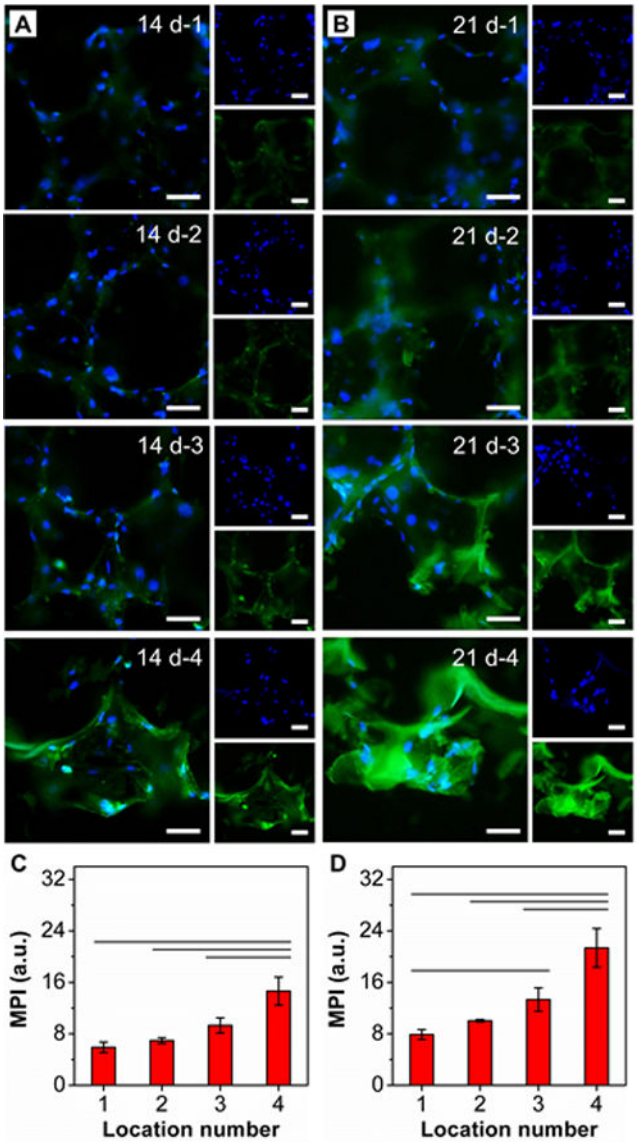

Figure 5.

OCN staining of ASCs seeded in the HAp-graded PLGA inverse opal scaffold after (A) 14 and (B) 21 days of culture at locations 1, 2, 3, and 4. Nuclei were stained with DAPI and shown in blue and OCN is shown in green. Scale bars: 50 μm. C, D) MPI analysis of OCN corresponding to images such as those shown in (A) and (B) ($n = 3$). Significant differences are indicated by lines over the bars ($p < 0.05$).

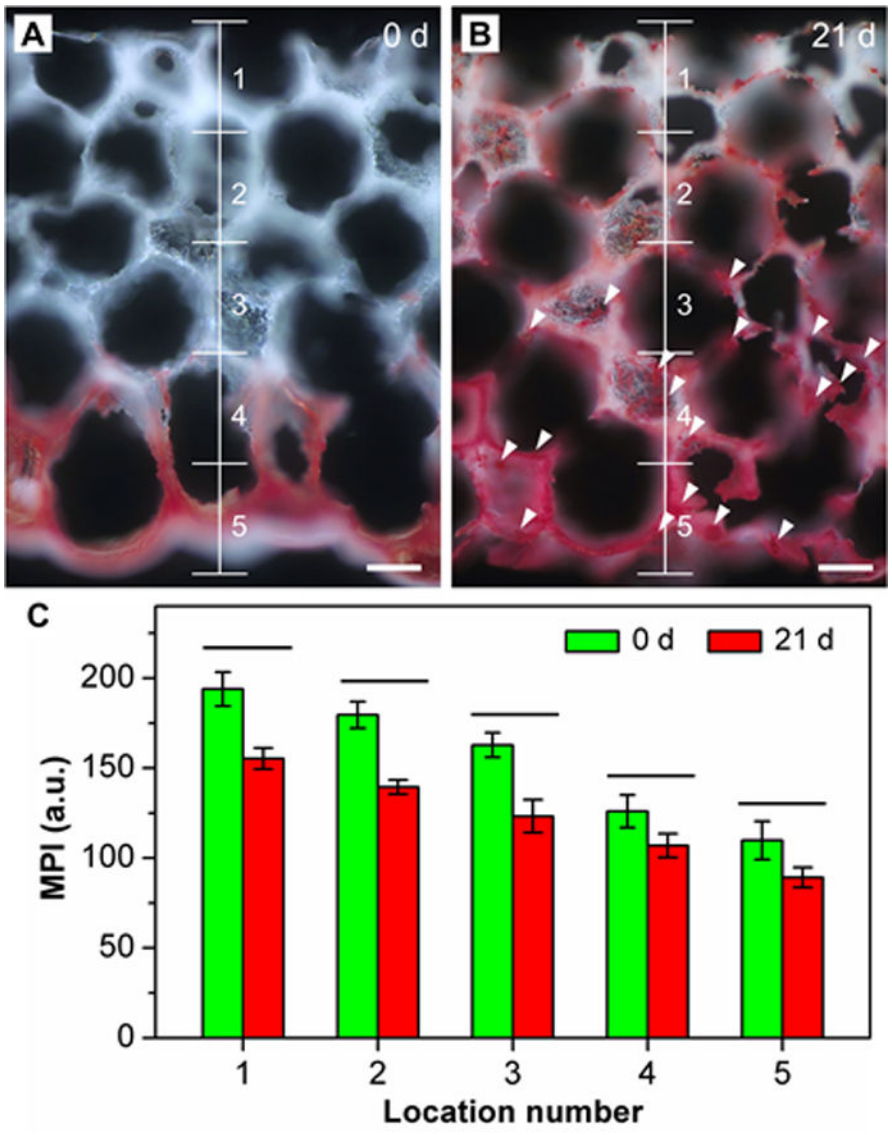

Figure 6.

Dark-field images of Alizarin Red S staining of calcium deposition on the ASC-seeded HAp-graded scaffold after A) 0 and B) 21 days of culture. White arrowheads indicate the calcium nodules. Scale bars: 100 μm. C) MPI analysis of the images such as those shown in (A) and (B) ($n = 3$). Significant differences are indicated by lines over the bars ($p < 0.05$).

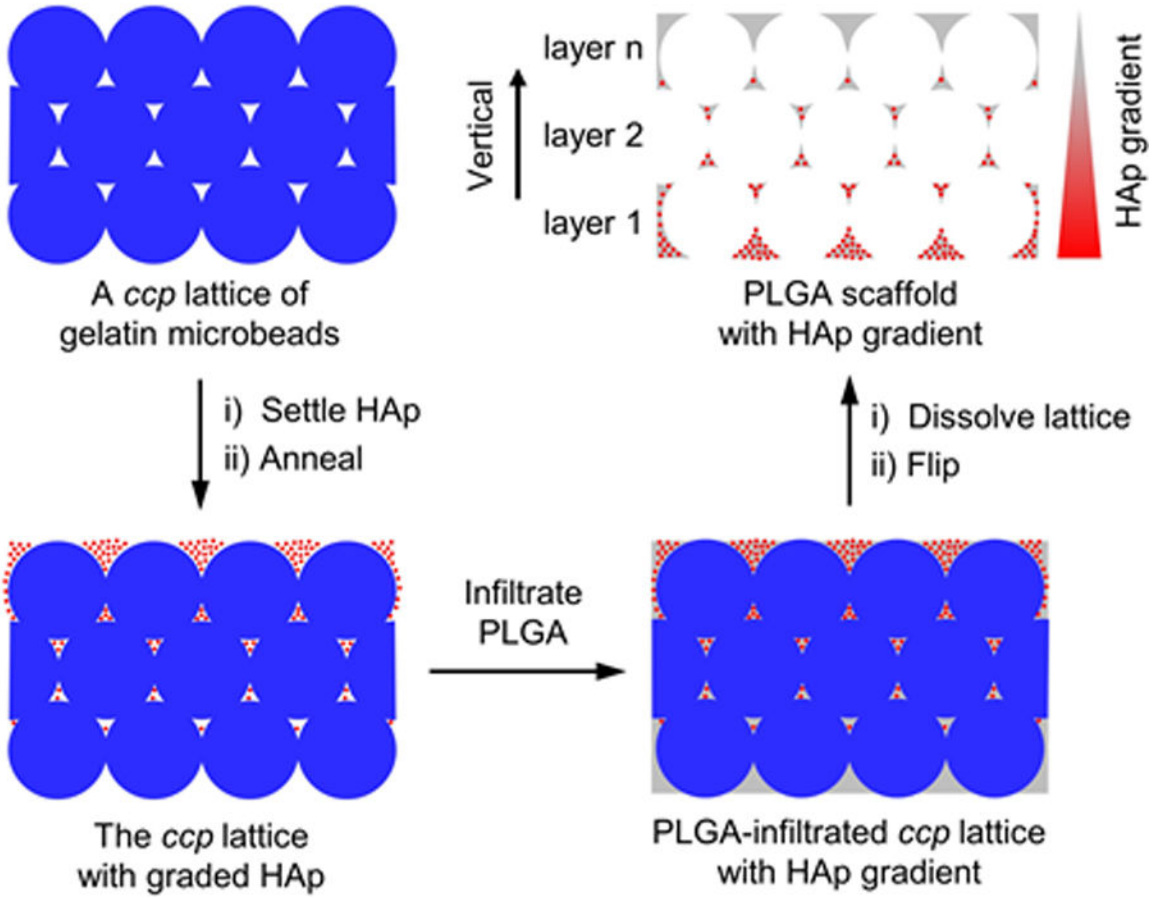

Scheme 1.

Schematic illustration showing the generation of a mineral gradient in a PLGA inverse opal scaffold through sedimentation of HAp nanoparticles in a *ccp* lattice of gelatin microbeads, followed by fixation with PLGA matrix.